CHAPTER 4

Bioconvective EMHD Hybrid Nanofluid Flow Past a Stretching Sheet *

4.1 INTRODUCTION

Heat and mass transfer due to stretching sheets plays a significant role in many aspects of engineering and industrial field such as metal spinning and drawing plastic films, glass blowing, crystal growing, cooling of filaments, and textiles, etc.

This chapter includes a theoretical investigation of bioconvective electromagnetohydrodynamic (EMHD) hybrid nanofluid (water-based $CNT - Fe_3O_4$) over a stretching surface. The impact of viscous dissipation, chemical reaction, and stratification is also explored in it. Governing nonlinear partial differential equations are transformed into ordinary differential equations with similarity transformation and treated numerically using bvp4c in MATLAB software. The drag coefficient has been statistically scrutinized utilizing the four-factor response surface methodology.

4.2 MATHEMATICAL FORMULATION

Consider a steady two-dimensional bioconvective flow past a linearly stretching sheet (with velocity $u_w(x) = cx$) placed along the x-axis (see Figure 4.1). The

*Published in Waves in Random and Complex Media (Taylor & Francis), 2022;(*early access)*

water-based carbon nanotube nanofluid embodied with microorganisms occupies the region $y > 0$. An external electric field (of intensity E_0) and an external magnetic field (of magnetic strength B_0) are applied perpendicular to the fluid flow. The induced magnetic field was ignored due to the supposition of a small magnetic Reynolds number. Chemical reaction, viscous dissipation, and stratification effects are also incorporated. Using the Tiwari-Das nanoliquid model (see (Tiwari & Das, 2007)), the governing equations take the form (see (Alsaedi et al., 2017),(Bilal, 2020), (Daniel, Aziz, Ismail, & Bahar, 2020)):

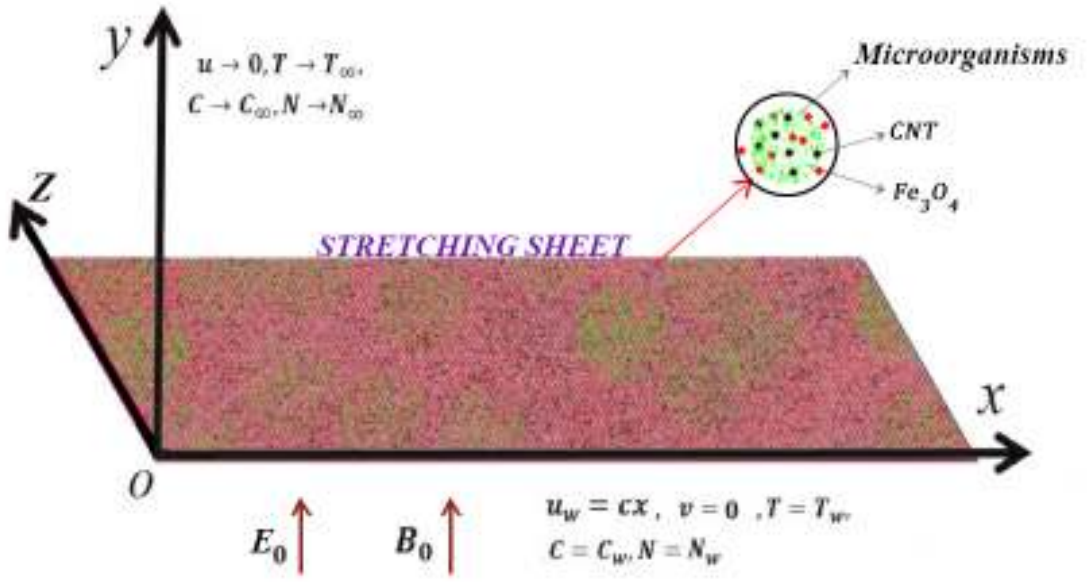

Figure 4.1: *Physical configuration*

$$\frac{\partial u}{\partial x} + \frac{\partial v}{\partial y} = 0 \tag{4.2.1}$$

$$u\frac{\partial u}{\partial x} + v\frac{\partial u}{\partial y} = \left(\frac{\mu_{hnf}}{\rho_{hnf}}\right)\frac{\partial^2 u}{\partial y^2} + \frac{\sigma_{hnf}}{\rho_{hnf}}\left(E_0 B_0 - B_0^2 u\right) \tag{4.2.2}$$

$$u\frac{\partial T}{\partial x} + v\frac{\partial T}{\partial y} = \alpha_{hnf}\frac{\partial^2 T}{\partial y^2} + \frac{\mu_{hnf}}{(\rho C_p)_{hnf}}\left(\frac{\partial u}{\partial y}\right)^2 \tag{4.2.3}$$

$$u\frac{\partial C}{\partial x} + v\frac{\partial C}{\partial y} = D_B\frac{\partial^2 C}{\partial y^2} - K_0\left(C - C_\infty\right) \tag{4.2.4}$$

$$u\frac{\partial N}{\partial x}+v\frac{\partial N}{\partial y}+\frac{bW_c}{C_w-C_0}\left(\frac{\partial}{\partial y}\left(N\frac{\partial C}{\partial y}\right)\right)=\ D_m\frac{\partial^2 N}{\partial y^2} \tag{4.2.5}$$

subject to the boundary constraints

$$\left.\begin{array}{c} u=u_w\left(x\right)=cx,\ v=0,\ T=T_w=T_0+\delta_1 x, \\ C=C_w=C_0+\varepsilon_1 x,\ N=N_w=N_0+\xi_1 x \end{array}\right\} \text{at} y=0 \tag{4.2.6}$$

$$\left.\begin{array}{c} u\to 0,\ T\to T_\infty=T_0+\delta_2 x,\ C\to C_\infty=C_0+\varepsilon_2 x, \\ N\to N_\infty=N_0+\xi_2 x \end{array}\right\} \text{as} y\to\infty \tag{4.2.7}$$

where δ_i, ε_i and ξ_i $(i=1,2)$ are dimensional constants.

The hybrid nanofluid models utilized in the current problem are (see (Sreedevi & Reddy, 2019), (Tulu & Ibrahim, 2020), (Saba, Ahmed, Khan, & Mohyud-Din, 2019)):

Effective Dynamic Viscosity:

$$\frac{\mu_{hnf}}{\mu_f}=\frac{1}{\left(1-\phi_1\right)^{2.5}\left(1-\phi_2\right)^{2.5}}=\frac{1}{A_1}$$

Effective Density:

$$\frac{\rho_{hnf}}{\rho_f}=\left(1-\phi_2\right)\left[1-\phi_1+\phi_1\left(\frac{\rho_{s_1}}{\rho_f}\right)\right]+\ \phi_2\left(\frac{\rho_{s_2}}{\rho_f}\right)=A_2$$

Effective Specific Heat:

$$\frac{\left(\rho C_p\right)_{hnf}}{\left(\rho C_p\right)_f}=\left(1-\phi_2\right)\left[1-\phi_1+\phi_1\left(\frac{\left(\rho c_p\right)_{s_1}}{\left(\rho c_p\right)_f}\right)\right]+\ \phi_2\left(\frac{\left(\rho c_p\right)_{s_2}}{\left(\rho c_p\right)_f}\right)=A_3$$

Effective Thermal Conductivity:

$$\frac{K_{hnf}}{K_f}=A_4, where$$

$$\frac{K_{hnf}}{K_{nf}}=\frac{1-\phi_2+2\phi_2\left(\frac{K_{s_2}}{K_{s_2}-K_{nf}}\right)\ln\left(\frac{K_{s_2}+K_{nf}}{2K_{nf}}\right)}{1-\phi_2+2\phi_2\left(\frac{K_{nf}}{K_{s_2}-K_{nf}}\right)\ln\left(\frac{K_{s_2}+K_{nf}}{2K_{nf}}\right)}$$

and

$$\frac{K_{nf}}{K_f}=\frac{K_{s_1}+2K_f-2\phi_1\left(K_f-K_{s_1}\right)}{K_{s_1}+2K_f+\phi_1\left(K_f-K_{s_1}\right)}$$

Effective Electrical Conductivity:

$$\frac{\sigma_{hnf}}{\sigma_f} = 1 + \frac{3\left(\frac{\phi_1\sigma_1+\phi_2\sigma_2}{\sigma_f} - (\phi_1+\phi_2)\right)}{2+\left(\frac{\phi_1\sigma_1+\phi_2\sigma_2}{(\phi_1+\phi_2)\sigma_f}\right) - \left(\frac{\phi_1\sigma_1+\phi_2\sigma_2}{\sigma_f} - (\phi_1+\phi_2)\right)} = A_5$$

Consider the following similarity transformations (reffered from (Alsaedi et al., 2017) and (Bilal, 2020):

$$\left.\begin{array}{l} u = cxf'(\eta)\,,\ v = -\sqrt{c\vartheta_f}\ f(\eta)\,,\ \eta = y\sqrt{\frac{c}{\vartheta_f}}\ , \\ \theta(\eta) = \frac{T-T_\infty}{T_w-T_0},\ \psi(\eta) = \frac{C-C_\infty}{C_w-C_0},\ \chi(\eta) = \frac{N-N_\infty}{N_w-N_0} \end{array}\right\} \tag{4.2.8}$$

Introducing these similarity variables and hybrid nanofluid constants the governing equations along with the boundary conditions are transmuted to:

$$f''' + A_1\ A_2\ f\ f'' - (A_1\ A_5\ H + A_1\ A_2\ f')\, f' + A_1\ A_5\ H\ E = 0 \tag{4.2.9}$$

$$A_4\ \theta'' + A_3\ Pr\ f\ \theta' + \frac{\mathrm{Pr}\, Ec}{A_1}(f'')^2 = 0 \tag{4.2.10}$$

$$\psi'' + Le\ f\ \psi' - Le\ K_c\ \psi = 0 \tag{4.2.11}$$

$$\chi'' + (f\ Lb - Pe\ \psi')\,\chi' - Pe\ \psi''\chi - Pe\ \Omega\psi'' = 0 \tag{4.2.12}$$

with

$$f(0) = 0\ ,\ f'(0) = 1\ ,\ \theta(0) = 1 - S_1\ ,\ \psi(0) = 1 - S_2\ ,\ \chi(0) = 1 - S_3 \tag{4.2.13}$$

$$f'(\infty) \to 0,\quad \theta(\infty) = 0,\quad \psi(\infty) \to 0,\quad \chi(\infty) \to 0 \quad as\ \eta \to \infty \tag{4.2.14}$$

4.3 PHYSICAL QUANTITIES

The physical quantities in non-dimensional form are given by:

Drag coefficient:

$$Cf_x = \frac{\mu_{hnf}\left(\frac{\partial u}{\partial y}\right)_{y=0}}{\rho_f (u_w)^2} \ \Rightarrow\ Re_x^{1/2} Cf_x = \frac{f''(0)}{A_1} \tag{4.3.1}$$

Local Nusselt number:

$$Nu_x = -\frac{xK_{hnf}\left(\frac{\partial T}{\partial y}\right)_{y=0}}{K_f\,(T_w - T_0)} \Rightarrow Re_x^{-1/2} Nu_x = -A_4\theta'(0) \tag{4.3.2}$$

Local Sherwood number:

$$Sh_x = -\frac{xD_B\left(\frac{\partial C}{\partial y}\right)_{y=0}}{D_B\left(C_w - C_0\right)} \Rightarrow Re_x^{-1/2} Sh_x = -\psi'(0) \tag{4.3.3}$$

Local microorganism density number:

$$Nn_x = -\frac{xD_m\left(\frac{\partial N}{\partial y}\right)_{y=0}}{D_m\left(N_w - N_0\right)} \Rightarrow Re_x^{-1/2} Nn_x = -\chi'(0) \tag{4.3.4}$$

where $Re_x = \frac{u_w x}{\vartheta_f}$ is the local Reynold's number.

4.4 NUMERICAL PROCEDURE AND VALIDATION

Since equations (4.2.9) to (4.2.12) are highly nonlinear, it is very hard to find a closed-form or an exact solution. Hence an approximate solution is computed numerically by employing the bvp4c algorithm (a finite difference-based built-in numerical procedure) in MATLAB. For this purpose, let

$$f = \Upsilon_1\ ,\ f' = \Upsilon_2\ ,\ f'' = \Upsilon_3\ ,\ f''' = \Upsilon_3'\ ,\ \theta = \Upsilon_4\ ,\ \theta' = \Upsilon_5\ ,\ \theta'' = \Upsilon_5'\ ,$$
$$\psi = \Upsilon_6\ ,\ \psi' = \Upsilon_7\ ,\ \psi'' = \Upsilon_7'\ ,\ \chi = \Upsilon_8\ ,\ \chi' = \Upsilon_9\ ,\ \chi'' = \Upsilon_9'.$$

The transmuted system of first-order ODEs are given as:

$$\Upsilon_1' = \Upsilon_2 \tag{4.4.1}$$

$$\Upsilon_2' = \Upsilon_3 \tag{4.4.2}$$

$$\Upsilon_3' = \left(A_1\ A_5\ H + A_1\ A_2\ \Upsilon_2\right)\Upsilon_2 - A_1\ A_2\ \Upsilon_1\ \Upsilon_3 - A_1\ A_5\ H\ E \tag{4.4.3}$$

$$\Upsilon_4' = \Upsilon_5 \tag{4.4.4}$$

$$\Upsilon_5{}' = -\frac{\left(A_1\ A_3\ Pr\ \Upsilon_1\ \Upsilon_5 + \Pr Ec\ \Upsilon_3^2\right)}{A_1 A_4} \tag{4.4.5}$$

$$\Upsilon_6' = \Upsilon_7 \tag{4.4.6}$$

$$\Upsilon_7' = Le\ K_c\ \Upsilon_6 - Le\ \Upsilon_1\ \Upsilon_7 \tag{4.4.7}$$

$$\Upsilon_8' = \Upsilon_9 \tag{4.4.8}$$

$$\Upsilon_9' = \left(\Upsilon_8 + \Omega\right) Pe\ \Upsilon_7{}' - \left(Lb\ \Upsilon_1 - Pe\ \Upsilon_7\right)\Upsilon_9 \tag{4.4.9}$$

with

$$\Upsilon_1(0) = 0, \quad \Upsilon_2(0) = 1, \quad \Upsilon_4(0) = 1 - S_1, \quad \Upsilon_6(0) = 1 - S_2, \quad \Upsilon_8(0) = 1 - S_3 \tag{4.4.10}$$

$$\Upsilon_2(\infty) = 0, \quad \Upsilon_4(\infty) = 0, \quad \Upsilon_6(\infty) = 0, \quad \Upsilon_8(\infty) = 0 \tag{4.4.11}$$

The bvp4c algorithm uses a three-stage Lobatto IIIa formula built on an association polynomial that returns a C^1-continuous solution which is uniformly accurate to the fourth-order. The accuracy of the code and the validation of the current problem have been determined through a restrictive comparison with (W. Khan & Pop, 2010) (see Table 4.1).

4.5 RESULTS AND DISCUSSION

The upshot of effectual parameters on the physical quantities, microbial concentration profile ($\chi(\eta)$), nanofluid temperature profile ($\theta(\eta)$), velocity profile ($f'(\eta)$), and nanofluid concentration profile ($\psi(\eta)$) for $SWCNT-Fe_3O_4$ and $MWCNT-Fe_3O_4$ hybrid nanofluids has been depicted through Figures 4.2 - 4.20. The Prandtl number, Lewis number, bioconvection Lewis number, and infinity are fixed at 6.2, 2, 1.2, and 5, respectively. In addition, the thermophysical properties of the base fluid and the nanoparticles are identified in Table 4.2.

The Lorentz force produced in the presence of a magnetic field acts as a resistive force that clashes with the fluid motion and hence reduces the velocity. This decline in the velocity profile with improving Hartmann number (H), in the absence of an electric field, is exhibited in Figure 4.2. However, in the presence of an electric field, the velocity profile speeds up with increasing H values (depicted in Figure 4.3). Physically, this is due to the domination exerted by the electric field on the magnetic field. Figure 4.4 delineates the positive impact of electric field parameter E on the velocity profile. Physically, an increase in E contributes more electric field strength that in turn accelerates the fluid flow (see (Nayak, Mabood, Dogonchi, & Khan, 2021)). Further, it is noted that the velocity profile is minimum for the water-based $SWCNT - Fe_3O_4$ hybrid nanofluid.

The negative impact of thermal stratification parameter (S_1) on $\theta(\eta)$ is expressed in Figure 4.5. This is because the temperature variation between the ambient and fluid surface diminishes with augmenting S_1 values. Figure 4.6 deliberates

the consequence of Eckert number (Ec) on the nanofluid temperature. The elevation in the nanoliquid temperature is physically associated with the production of frictional energy caused by the collision of fluid particles. Figures 4.7 and 4.8 elucidate the improvement in $\theta(\eta)$ with augmenting volume fraction of CNT nanoparticle (ϕ_1) and volume fraction of Fe_3O_4 nanoparticle (ϕ_2) values, respectively. Physically, it is associated with the improvement in the thermal conductivity of the nanofluid occurring due to the increased nanoparticle occupancy. Moreover, a higher nanofluid temperature is observed for water-based $SWCNT - Fe_3O_4$ hybrid nanofluid.

The effect of chemical reaction parameter (K_c) and the solutal stratification parameter (S_2) on the concentration profile has been depicted in Figures 4.9 and 4.10, respectively. A decline in $\psi(\eta)$ is noted for increasing K_c and S_2 values. Physically, higher values of K_c expedite the nanoparticle consumption causing a drop in the concentration profile. Further, an augmentation in S_2 descends the volumetric fraction between the surface and reference nanoparticles, hence reducing the concentration profile.

Figure 4.11 illustrates the decreasing nature of $\chi(\eta)$ with augmenting microorganism density stratification parameter (S_3) values. This decline in the volumetric fraction can be physically attributed to the fact that increasing S_3 values descend the concentration difference of microorganisms between the surface and away from the surface.

Figures 4.12 - 4.15 explore the concurrent influence of effective parameters on surface drag and heat transfer rate. From Figures 4.12 and 4.13, it is noticed that the drag coefficient ascends with E and descends with ϕ_1, ϕ_2, and H. Also, it is observed that the heat transfer rate descends with augmenting ϕ_2, Ec and S_1 values (see Figures 4.14 and 4.15). Further, it is noted that the water-based $SWCNT - Fe_3O_4$ hybrid nanofluid exhibits the least surface drag and the highest heat transfer rate.

Tables 4.3 and 4.4 elucidate the impact of pertinent parameters on the mass transfer rate and the microorganism density number. Further, the slope of linear regression is calculated to statistically investigate the trend of variation over the physical quantities. The magnitude of slope represents the rate of change of considered physical quantity per unit value of the corresponding parameter and the sign of slope symbolizes the nature of this impact. The key observations drawn from

Tables 4.3 and 4.4 are:

- The mass transfer rate is a decreasing function of H and an increasing function of E and K_c.
- The water-based $MWCNT - Fe_3O_4$ hybrid nanofluid exhibits the highest mass transfer rate in comparison with water-based $SWCNT - Fe_3O_4$ hybrid nanofluid.
- A decrement rate of 166.70% (for $SWCNT - Fe_3O_4$ case) and 166.80% (for$MWCNT - Fe_3O_4$ case) are observed on the mass transfer rate when the value of solutal stratification parameter is augmented.
- The microorganism density number is a decreasing function of H and an increasing function of E and K_c.
- The microorganism density number for water-based $MWCNT-Fe_3O_4$ hybrid nanofluid is higher than the water-based $SWCNT - Fe_3O_4$ hybrid nanofluid.
- The microorganism density number descends at a rate of 124.60% (for $SWCNT-Fe_3O_4$ case) and 124.90% (for $MWCNT - Fe_3O_4$ case) when the value of microorganism density stratification parameter is increased.

4.6 STATISTICAL ANALYSIS

4.6.1 Response Surface Methodology (RSM)

The response surface methodology (RSM) is a statistical mechanism to measure the level of interaction exerted by the pertinent parameters (independent variable) chosen on the response (dependent) variable and to optimize it. In this problem, the impact of nanoparticle volume fraction of carbon nanotubes ($0.01 \leq \phi_1 \leq 0.09$), the volume fraction of magnetite nanoparticles ($0.01 \leq \phi_2 \leq 0.09$), Hartmann number ($0.4 \leq M \leq 2$), and electric field parameter ($0.1 \leq E \leq 0.5$) on the drag coefficient ($Cf_x Re_x^{1/2}$) for both $SWCNT - Fe_3O_4$ and $MWCNT - Fe_3O_4$ hybrid nanofluids (named as Cf_{SWCNT} and Cf_{MWCNT}, respectively) are scrutinized statistically using a five-level four-factor response surface optimized model. The effectual parameters and their levels are charted in Table 4.5.

The four-factor response surface optimized model (espousing CCD) for response variables involving linear, quadratic, and interactive terms is couched by:

$$Response = b_0 + b_1\ A + b_2 B + b_3 C + b_4 D + b_5 A^2 + b_6 B^2 + b_7 C^2 + b_8 D^2 + b_9 AB + b_{10} AC + b_{11} AD + b_{12} BC + b_{13} BD + b_{14} CD \quad (4.6.1)$$

where $b_i (i = 0, 1...14)$ represent the regression coefficients. The experimental design and response for the 30 runs (in accordance with the four-factor CCD) are showcased in Table 4.6.

Tables 4.7 and 4.8 (ANOVA table) explain the efficiency of the approximated model. A parameter is asserted to be significant if the corresponding p-value is less than 0.05 and the corresponding F-value is greater than 1. It is noticed that the quadratic term in M is not significant for Cf_{SWCNT} and hence the term is deleted from the model. The coefficient of determination (R^2) for the model is estimated to be 99.98% which also boosts the model accuracy. The reliability and accuracy of the estimated models (Cf_{SWCNT} and Cf_{MWCNT}) and are further elucidated using residual versus fitted plots (see Figures 4.16 and 4.17). Furthermore, a maximum error of 0.006 can be noted from the fitted versus residual plot which also accounts for the correctness of the model.

The fitted quadratic models are given by:

$$Cf_{SWCNT} = -1.01558 - 2.70667\ \phi_1 - 3.78729\ \phi_2 - 0.388995\ H + 0.107104\ E - 4.49479\ {\phi_1}^2 - 4.58854\ {\phi_2}^2 - 0.116042\ E^2 - 6.90625\ \phi_1\ \phi_2\ - 0.831250\ \phi_1\ H + 3.31875\ \phi_1\ E - 0.642187\ \phi_2\ H\ + 2.98750\ \phi_2\ E\ + 0.654063\ H\ E \quad (4.6.2)$$

$$Cf_{MWCNT} = -1.01346 - 2.28813\ \phi_1 - 3.79583\ \phi_2 - 0.391698\ H + 0.104667\ E - 4.34375\ {\phi_1}^2 - 4.56250\ {\phi_2}^2 + 0.007734\ H^2 - 0.115000\ E^2 - 7.31250\ \phi_1\ \phi_2 - 0.906250\ \phi_1\ H\ + 3.45625\ \phi_1\ E - 0.637500\ \phi_2\ H\ + 2.98125\ \phi_2\ E\ + 0.655313\ H\ E \quad (4.6.3)$$

From equations (4.6.2) and (4.6.3), it can be inferred that ϕ_1, ϕ_2 and H reduce the surface drag (both cases) and E increase the surface drag (both cases). The simul-

taneous interaction of two parameters on the drag coefficient is delineated using surface plots (see Figures 4.18 and 4.19) by fixing the remaining two parameters at their corresponding medium level. From Figures 4.18 and 4.19, it is perceived that the surface drag (both cases) is highest for smaller values of ϕ_1, ϕ_2 and H and larger values of E.

4.7 CONCLUSION

The bioconvective electromagnetohydrodynamic hybrid nanoliquid flow due to a linearly elongating sheet has been theoretically investigated. The nanoliquid flow has been modeled using the Tiwari-Das model. The mathematically modeled equations are transmuted into a system of first-order ODEs using apposite similarity transformations and then resolved numerically with the aid of bvp4c (a finite difference-based built-in numerical procedure) in MATLAB. A comparative analysis of the hybrid nanoliquid flow using $SWCNT - Fe_3O_4$ and $MWCNT - Fe_3O_4$ nanoparticles has been carried out. Further, the influence of nanoparticle volume fraction of carbon nanotubes ($0.01 \leq \phi_1 \leq 0.09$), the volume fraction of magnetite nanoparticles ($0.01 \leq \phi_2 \leq 0.09$) , Hartmann number ($0.4 \leq H \leq 2$) , and electric field parameter ($0.1 \leq E \leq 0.5$) on the surface drag has been scrutinized utilizing the four-factor response surface optimized model. The major observations of the study are:

- The velocity profile ascends with augmenting electric field parameter values.
- The velocity profile is minimum for water-based $SWCNT - Fe_3O_4$ hybrid nanofluid.
- The surface drag coefficient is highest for smaller values of Hartmann number and larger values of electric field parameter.
- The volume fraction of nanoparticles and Eckert number intensifies the nanofluid temperature.
- A higher nanofluid temperature is observed for water-based $SWCNT-Fe_3O_4$ hybrid nanofluid.
- The solutal and microorganism density stratification parameters are negatively correlated with volume fraction and microbial concentration, respec-

tively.

- A decrement rate of 166.70% (for $SWCNT - Fe_3O_4$ case) and 166.80% (for $MWCNT - Fe_3O_4$ case) are observed on the mass transfer rate when the value of solutal stratification parameter is augmented.

- The microorganism density number descends at a rate of 124.60% (for $SWCNT - Fe_3O_4$ case) and 124.90% (for $MWCNT - Fe_3O_4$ case) when the value of microorganism density stratification parameter is increased.

- The fitted quadratic model for the drag coefficient of water-based $SWCNT - Fe_3O_4$ hybrid nanofluid is given by:

$$Cf_{SWCNT} = -1.01558 - 2.70667\,\phi_1 - 3.78729\,\phi_2 - 0.388995\,H + 0.107104\,E - 4.49479\,{\phi_1}^2 - 4.58854\,{\phi_2}^2 - 0.116042\,E^2 - 6.90625\,\phi_1\,\phi_2 - 0.831250\,\phi_1\,H + 3.31875\,\phi_1\,E - 0.642187\,\phi_2\,H + 2.98750\,\phi_2\,E + 0.654063\,H\,E$$

- The fitted quadratic model for the drag coefficient of water-based $MWCNT - Fe_3O_4$ hybrid nanofluid is given by:

$$Cf_{MWCNT} = -1.01346 - 2.28813\,\phi_1 - 3.79583\,\phi_2 - 0.391698\,H + 0.104667\,E - 4.34375\,{\phi_1}^2 - 4.56250\,{\phi_2}^2 + 0.007734\,H^2 - 0.115000\,E^2 - 7.31250\,\phi_1\,\phi_2 - 0.906250\,\phi_1\,H + 3.45625\,\phi_1\,E - 0.637500\,\phi_2\,H + 2.98125\,\phi_2\,E + 0.655313\,H\,E$$

TABLES AND GRAPHS

Table 4.1: *Comparison of* $Nu_x Re_x^{-1/2}$ *for differing* Pr *values when* $H = E = K_c = Ec = Le = Lb = Pe = \Omega = S_1 = S_2 = S_3 = 0$

Pr	(W. Khan & Pop, 2010)	**Present study**
0.7	0.4539	0.454
2	0.9113	0.9114
7	1.8954	1.8954
20	3.3539	3.3539
70	6.4621	6.4622

Table 4.2: *Thermophysical properties*

Physical Properties	ρ	C_p	k	σ
Pure water	997.1	4179	0.613	0.05
$SWCNT$	2600	425	6600	10^6
$MWCNT$	1600	796	3000	10^7
Fe_3O_4	5180	670	9.7	25000

Table 4.3: *Comparison of $Sh_x Re_x^{-1/2}$ for differing H, E, K_c, and S_2 values when $Le = 2, Lb = 1.2, Ec = 0.3, \Omega = Pe = 0.5, S_1 = S_3 = \phi_1 = \phi_2 = 0.1$ and $Pr = 6.2$*

H	E	K_c	S_2	$Sh_x Re_x^{-1/2}$	
				$SWCNT - Fe_3O_4$	$MWCNT - Fe_3O_4$
0.5				1.5105	1.5118
1				1.5003	1.5014
1.5				1.492	1.4929
Slope				**-0.0185**	**-0.0189**
	0.01			1.4989	1.5
	0.03			1.5003	1.5014
	0.05			1.5017	1.5028
Slope				**0.07**	**0.07**
		0.5		1.1913	1.1929
		1		1.5003	1.5014
		1.5		1.7538	1.7546
Slope				**0.5625**	**0.5617**
			0.05	1.5837	1.5848
			0.1	1.5003	1.5014
			0.15	1.417	1.418
Slope				**-1.667**	**-1.668**

Table 4.4: *Comparison of $Nn_xRe_x^{-1/2}$ for differing H, E, K_c, and S_3 values when $Le = 2, Lb = 1.2, Ec = 0.3, \Omega = Pe = 0.5, S_1 = S_2 = \phi_1 = \phi_2 = 0.1$ and $Pr = 6.2$*

H	E	K_c	S_3	$Nn_xRe_x^{-1/2}$	
				$SWCNT - Fe_3O_4$	$MWCNT - Fe_3O_4$
0.5				1.4584	1.4615
1				1.4346	1.4371
1.5				1.415	1.417
Slope				**-0.0434**	**-0.0445**
	0.01			1.4302	1.4327
	0.03			1.4346	1.4371
	0.05			1.4388	1.4413
Slope				**0.215**	**0.215**
		0.5		1.2325	1.2354
		1		1.4346	1.4371
		1.5		1.6021	1.6043
Slope				**0.3696**	**0.3689**
			0.05	1.4969	1.4995
			0.1	1.4346	1.4371
			0.15	1.3723	1.3746
Slope				**-1.246**	**-1.249**

Table 4.5: *Effectual parameter levels*

Parameter	**Symbol**	**Levels**				
		$-2(\alpha)$	**-1 (low)**	**0 (medium)**	**1 (high)**	$2(\alpha)$
ϕ_1	A	0.01	0.03	0.05	0.07	0.09
ϕ_2	B	0.01	0.03	0.05	0.07	0.09
H	C	0.4	0.8	1.2	1.6	2
E	D	0.1	0.2	0.3	0.4	0.5

Table 4.6: *Four-factor CCD experimental design and the corresponding responses*

Run	ϕ_1	ϕ_2	H	E	Response	
					Cf_{SWCNT}	Cf_{MWCNT}
1	0.03 (-1)	0.03 (-1)	0.8 (-1)	0.2 (-1)	-1.4092	-1.3978
2	0.07 (1)	0.03 (-1)	0.8 (-1)	0.2 (-1)	-1.5409	-1.5138
3	0.03 (-1)	0.07 (1)	0.8 (-1)	0.2 (-1)	-1.5813	-1.5705
4	0.07 (1)	0.07 (1)	0.8 (-1)	0.2 (-1)	-1.7237	-1.6979
5	0.03 (-1)	0.03 (-1)	1.6 (1)	0.2 (-1)	-1.6344	-1.6247
6	0.07 (1)	0.03 (-1)	1.6 (1)	0.2 (-1)	-1.7968	-1.774
7	0.03 (-1)	0.07 (1)	1.6 (1)	0.2 (-1)	-1.8309	-1.8218
8	0.07 (1)	0.07 (1)	1.6 (1)	0.2 (-1)	-2.0075	-1.9858
9	0.03 (-1)	0.03 (-1)	0.8 (-1)	0.4 (1)	-1.2542	-1.2421
10	0.07 (1)	0.03 (-1)	0.8 (-1)	0.4 (1)	-1.3663	-1.3375
11	0.03 (-1)	0.07 (1)	0.8 (-1)	0.4 (1)	-1.4091	-1.3977
12	0.07 (1)	0.07 (1)	0.8 (-1)	0.4 (1)	-1.5297	-1.5023
13	0.03 (-1)	0.03 (-1)	1.6 (1)	0.4 (1)	-1.3859	-1.3755
14	0.07 (1)	0.03 (-1)	1.6 (1)	0.4 (1)	-1.5176	-1.4928
15	0.03 (-1)	0.07 (1)	1.6 (1)	0.4 (1)	-1.5546	-1.5447
16	0.07 (1)	0.07 (1)	1.6 (1)	0.4 (1)	-1.6971	-1.6735
17	0.01 (-2)	0.05 (0)	1.2 (0)	0.3 (0)	-1.441	-1.4375
18	0.09 (2)	0.05 (0)	1.2 (0)	0.3 (0)	-1.7218	-1.6894
19	0.05 (0)	0.01 (-2)	1.2 (0)	0.3 (0)	-1.4028	-1.3842
20	0.05 (0)	0.09 (2)	1.2 (0)	0.3 (0)	-1.7603	-1.7434
21	0.05 (0)	0.05 (0)	0.4 (-2)	0.3 (0)	-1.3722	-1.3509
22	0.05 (0)	0.05 (0)	2 (2)	0.3 (0)	-1.7675	-1.7522
23	0.05 (0)	0.05 (0)	1.2 (0)	0.1 (-2)	-1.8089	-1.7924
24	0.05 (0)	0.05 (0)	1.2 (0)	0.5 (2)	-1.3488	-1.3298
25	0.05 (0)	0.05 (0)	1.2 (0)	0.3 (0)	-1.5739	-1.5562
26	0.05 (0)	0.05 (0)	1.2 (0)	0.3 (0)	-1.5739	-1.5562
27	0.05 (0)	0.05 (0)	1.2 (0)	0.3 (0)	-1.5739	-1.5562
28	0.05 (0)	0.05 (0)	1.2 (0)	0.3 (0)	-1.5739	-1.5562
29	0.05 (0)	0.05 (0)	1.2 (0)	0.3 (0)	-1.5739	-1.5562
30	0.05 (0)	0.05 (0)	1.2 (0)	0.3 (0)	-1.5739	-1.5562

Table 4.7: *ANOVA table* (Cf_{SWCNT}).

Source	**Deg. Of freedom**	**Adj. sum of squares**	**Adj. mean squares**	**F-value**	**p-value**
Model	14	0.8738	0.0624	8677.55	≤ 0.0001
ϕ_1	1	0.1178	0.1178	16380.5	≤ 0.0001
ϕ_2	1	0.1915	0.1915	26617.6	≤ 0.0001
H	1	0.2402	0.2402	33393.8	≤ 0.0001
E	1	0.3106	0.3106	43185.2	≤ 0.0001
$\phi_1 * \phi_1$	1	0.0001	0.0001	12.33	0.0032
$\phi_2 * \phi_2$	1	0.0001	0.0001	12.85	0.0027
$H * H$	1	0	0	**4.53**	**0.0504**
$E * E$	1	0	0	5.13	0.0387
$\phi_1 * \phi_2$	1	0.0001	0.0001	16.98	0.0009
$\phi_1 * H$	1	0.0007	0.0007	98.37	≤ 0.0001
$\phi_1 * E$	1	0.0007	0.0007	98	≤ 0.0001
$\phi_2 * H$	1	0.0004	0.0004	58.71	≤ 0.0001
$\phi_2 * E$	1	0.0006	0.0006	79.41	≤ 0.0001
$H * E$	1	0.011	0.011	1522.55	≤ 0.0001
Error	15	0.0001	$7.193 * 10^{-6}$		
Lack-of-Fit	10	0.0001	0	*	*
Pure Error	5	0	0		
Total	29	0.8739			
$R^2 = 0.9999$			Adjusted $R^2 = 0.9998$		

Table 4.8: *ANOVA table* (Cf_{MWCNT})

Source	**Deg. Of freedom**	**Adj. sum of squares**	**Adj. mean squares**	**F-value**	**p-value**
Model	14	0.8632	0.0617	8557.46	≤ 0.0001
ϕ_1	1	0.0946	0.0946	13126.3	≤ 0.0001
ϕ_2	1	0.1934	0.1934	26840.9	≤ 0.0001
H	1	0.2472	0.2472	34310.6	≤ 0.0001
E	1	0.3141	0.3141	43586.9	≤ 0.0001
$\phi_1 * \phi_1$	1	0.0001	0.0001	11.49	0.004
$\phi_2 * \phi_2$	1	0.0001	0.0001	12.68	0.0028
$H * H$	1	0	0	5.83	0.029
$E * E$	1	0	0	5.03	0.0404
$\phi_1 * \phi_2$	1	0.0001	0.0001	19	0.0006
$\phi_1 * H$	1	0.0008	0.0008	116.72	≤ 0.0001
$\phi_1 * E$	1	0.0008	0.0008	106.11	≤ 0.0001
$\phi_2 * H$	1	0.0004	0.0004	57.76	≤ 0.0001
$\phi_2 * E$	1	0.0006	0.0006	78.95	≤ 0.0001
$H * E$	1	0.011	0.011	1525.78	≤ 0.0001
Error	15	0.0001	$7.205 * 10^{-6}$		
Lack-of-Fit	10	0.0001	0	*	*
Pure Error	5	0	0		
Total	29	0.8633			
$R^2 = 0.9999$			Adjusted $R^2 = 0.9998$		

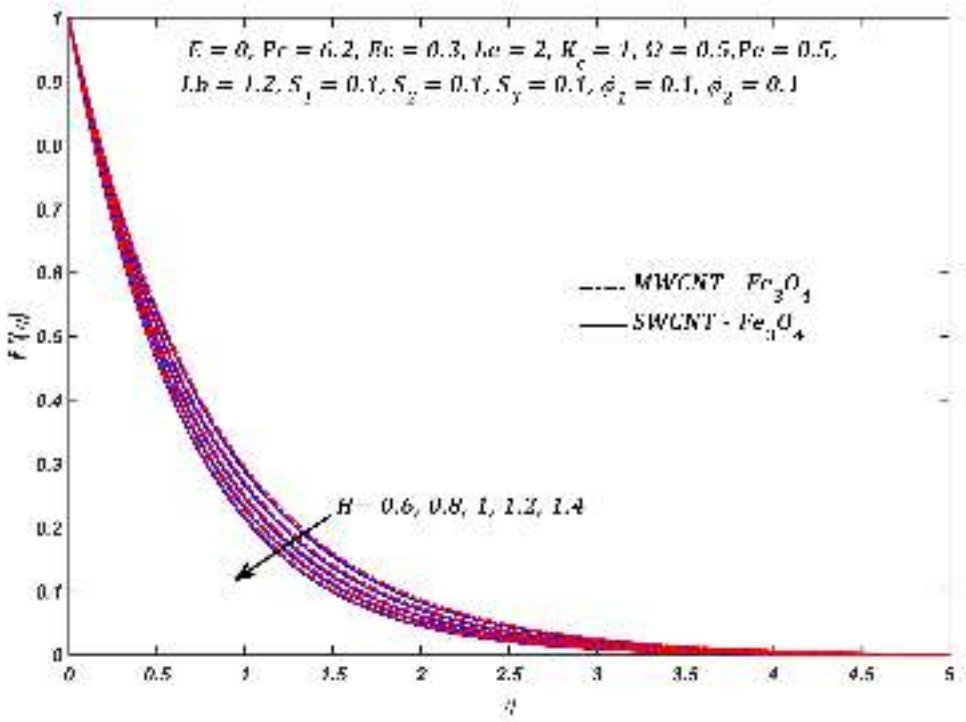

Figure 4.2: *Variation in* $f'(\eta)$ *with* H *when* $E = 0$

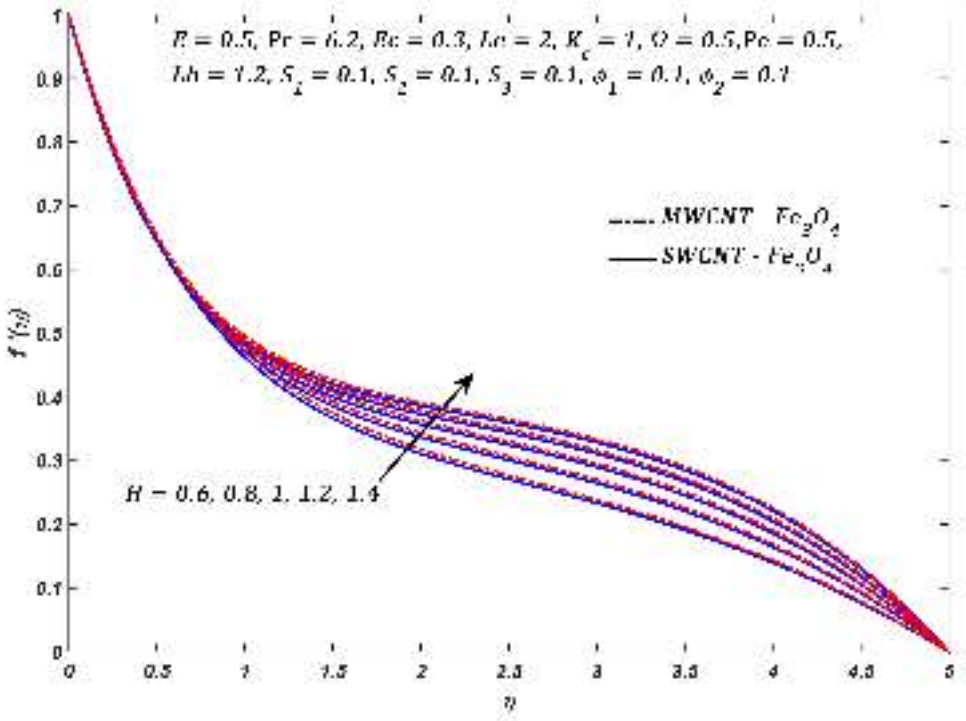

Figure 4.3: *Variation in* $f'(\eta)$ *with* H *when* $E \neq 0$

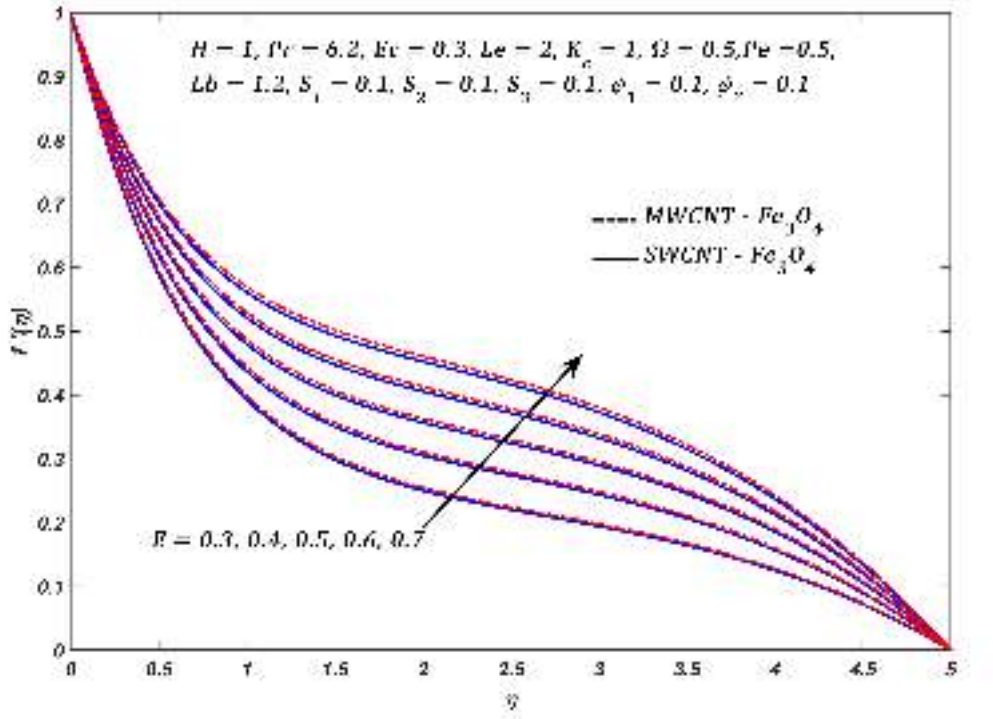

Figure 4.4: *Variation in* $f'(\eta)$ *with* E

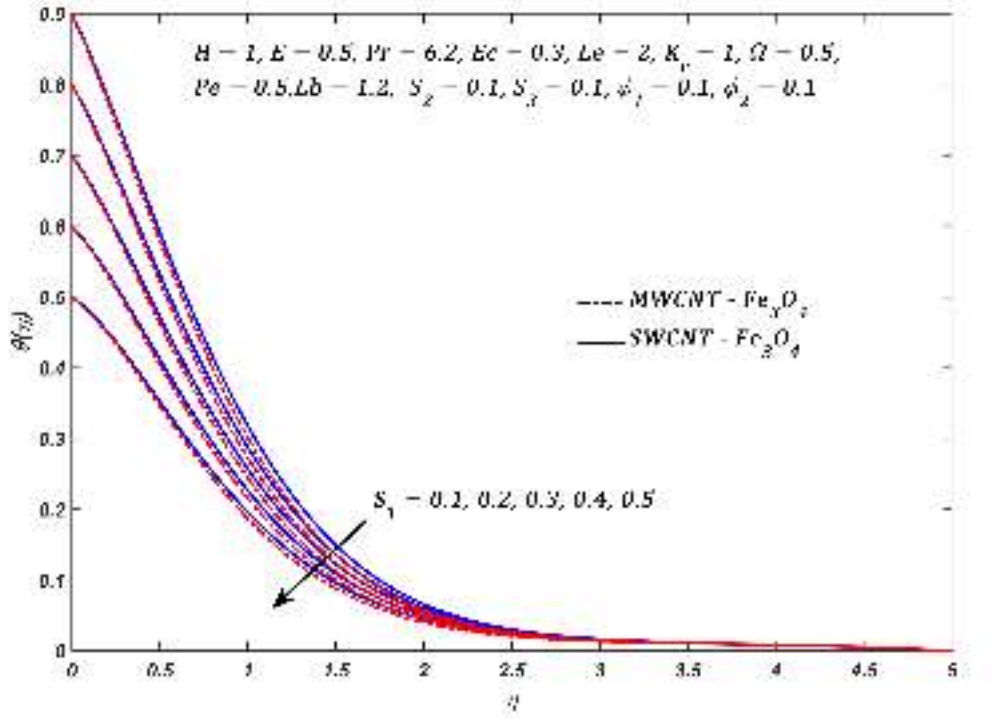

Figure 4.5: *Variation in* $\theta(\eta)$ *with* S_1

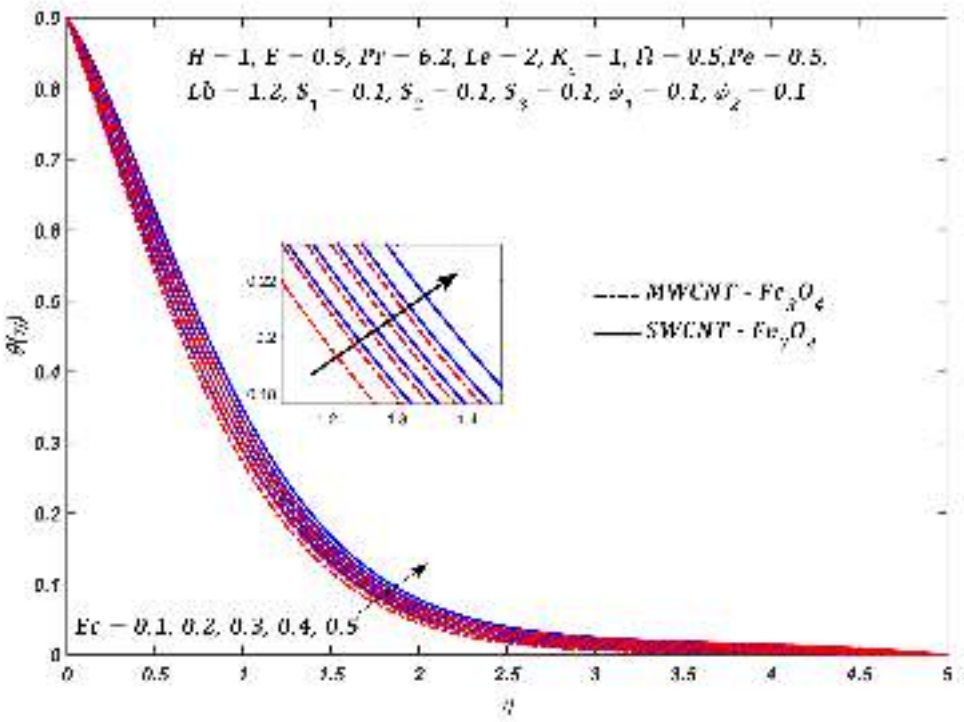

Figure 4.6: *Variation in* $\theta(\eta)$ *with* Ec

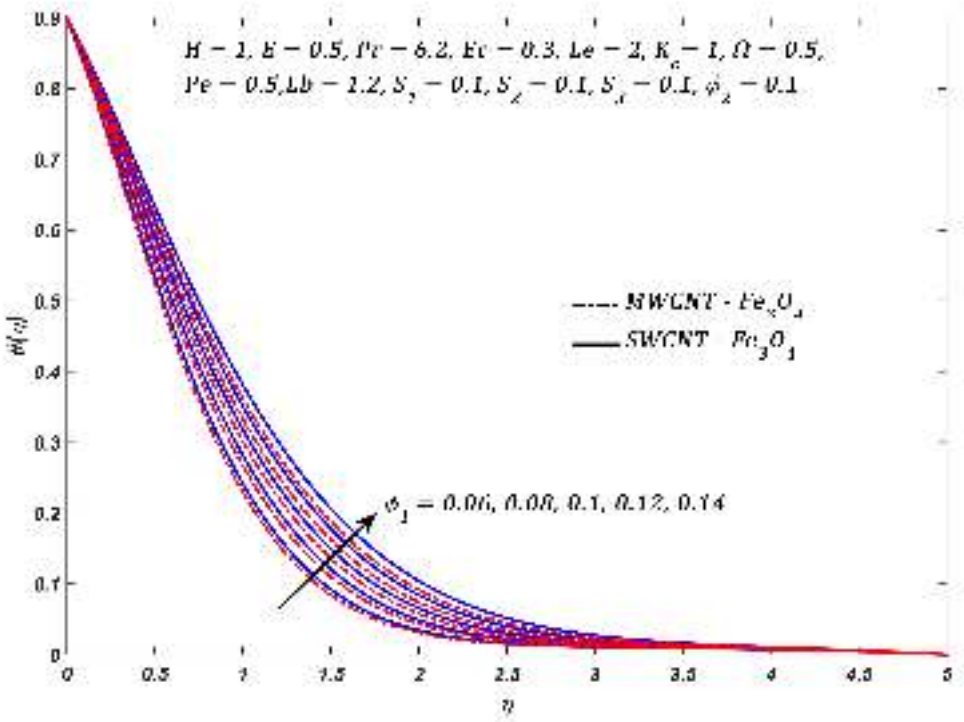

Figure 4.7: *Variation in* $\theta(\eta)$ *with* ϕ_1

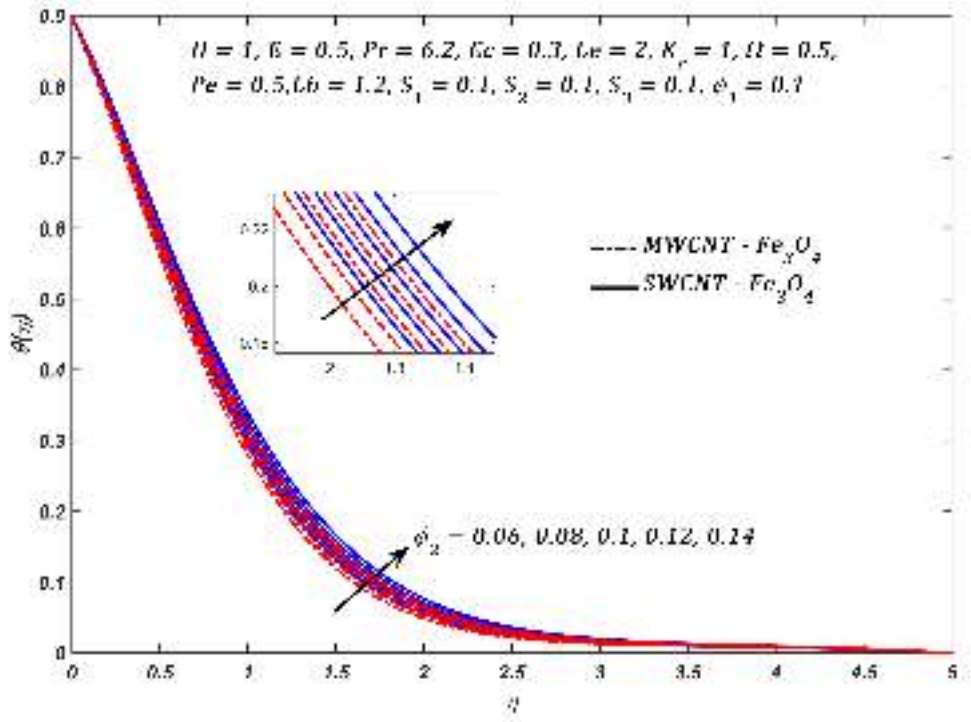

Figure 4.8: *Variation in* $\theta(\eta)$ *with* ϕ_2

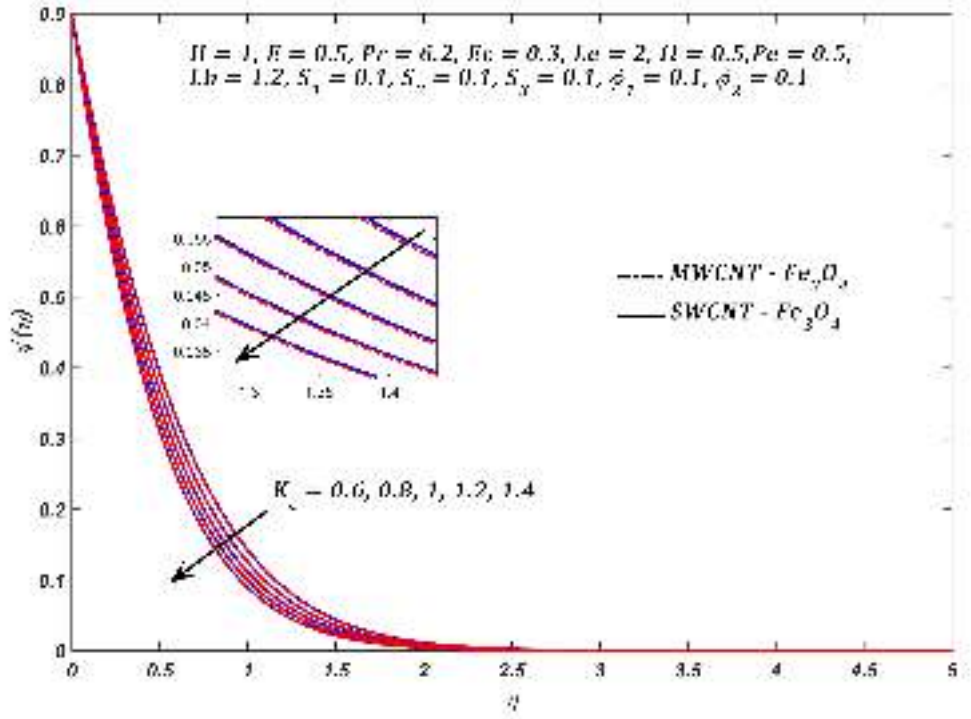

Figure 4.9: *Variation in* $\psi(\eta)$ *with* K_c

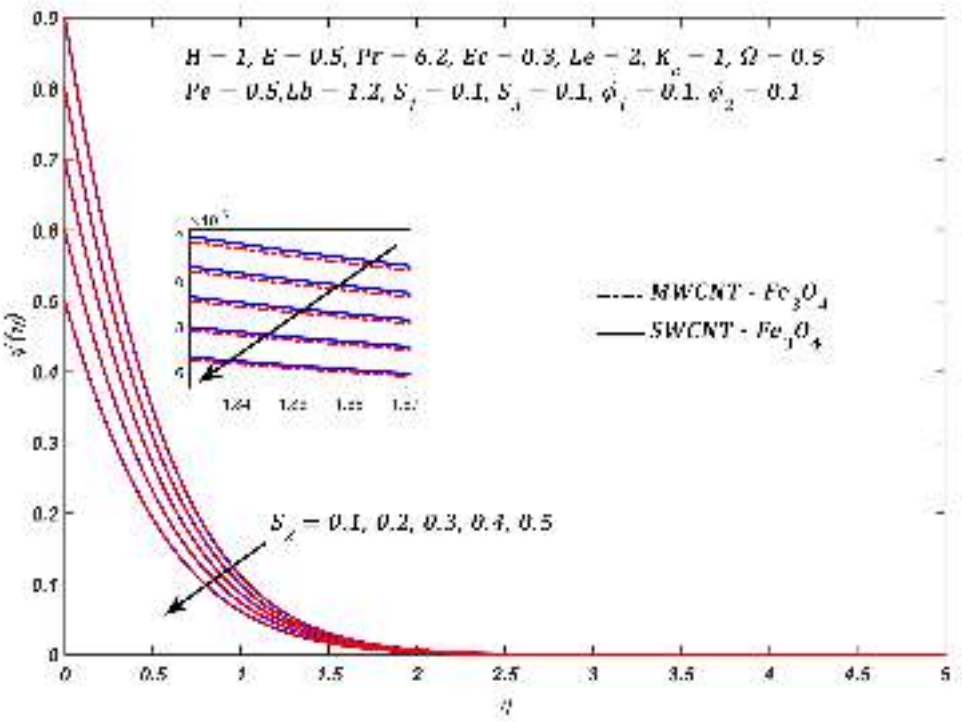

Figure 4.10: *Variation in* $\psi(\eta)$ *with* S_2

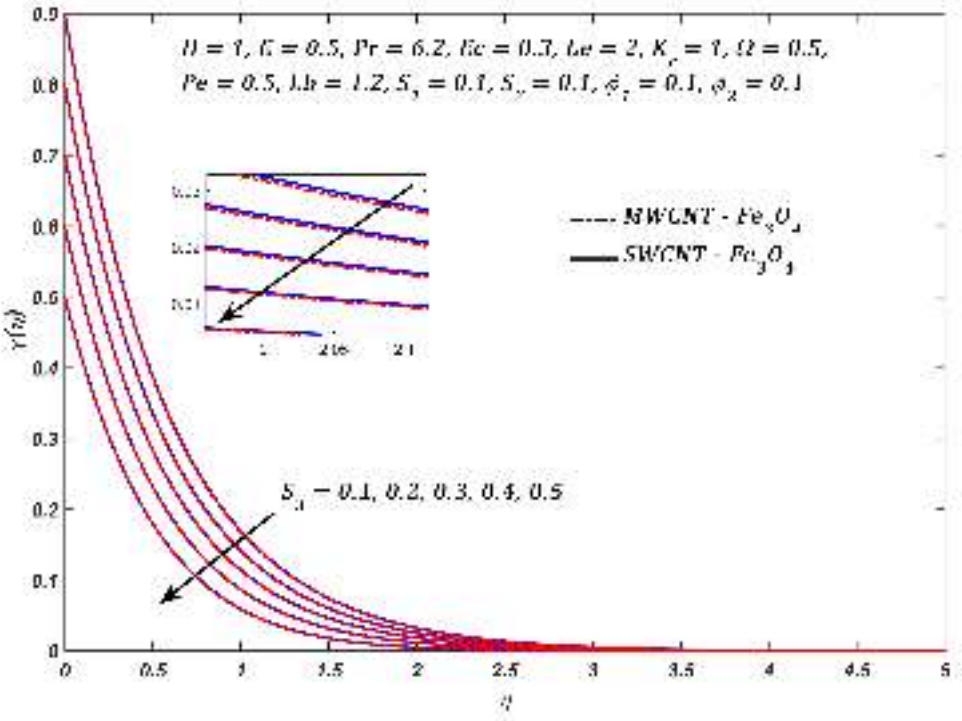

Figure 4.11: *Variation in* $\chi(\eta)$ *with* S_3

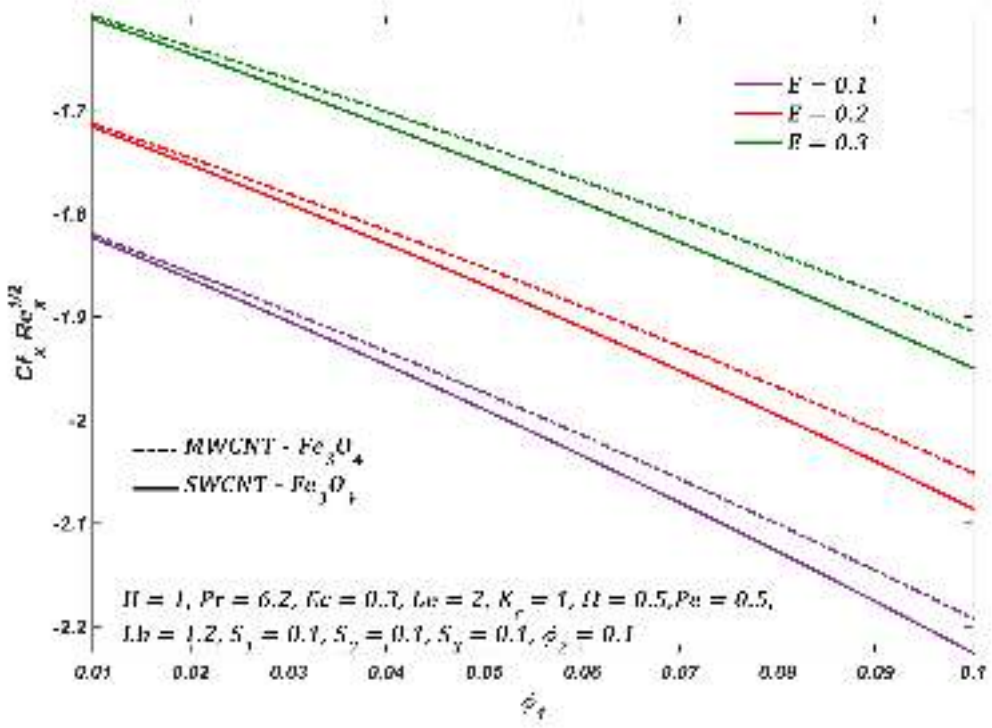

Figure 4.12: *Variation in* $Cf_x Re_x^{1/2}$ *with* ϕ_1 *and* E

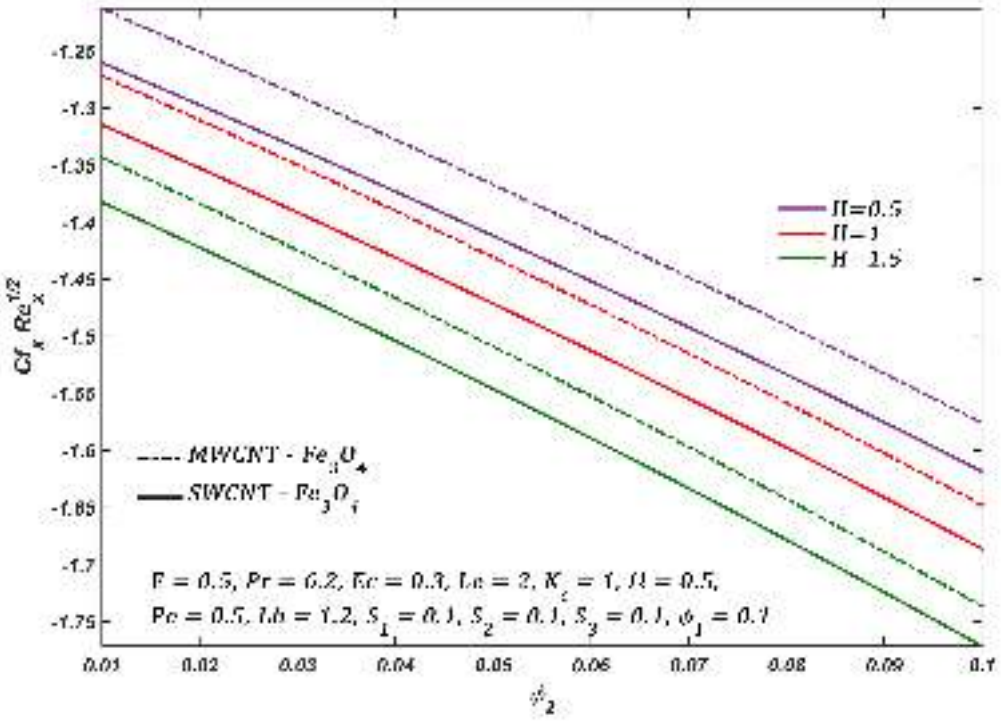

Figure 4.13: *Variation in* $Cf_x Re_x^{1/2}$ *with* ϕ_2 *and* M

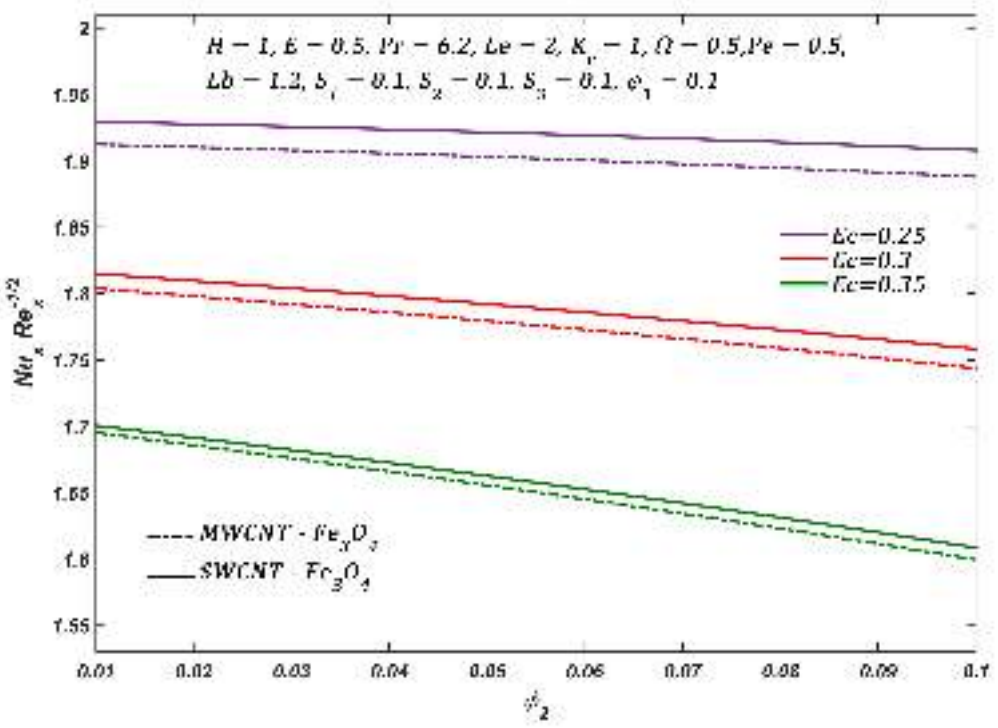

Figure 4.14: *Variation in* $Nu_x Re_x^{-1/2}$ *with* ϕ_2 *and* Ec

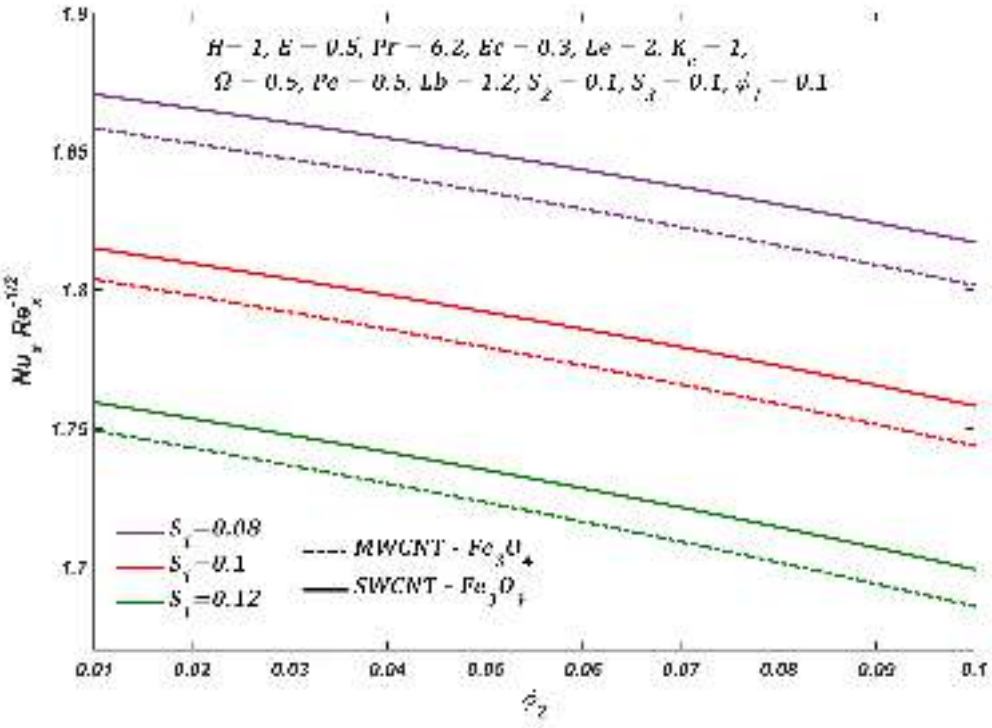

Figure 4.15: *Variation in* $Nu_x Re_x^{-1/2}$ *with* ϕ_2 *and* S_1

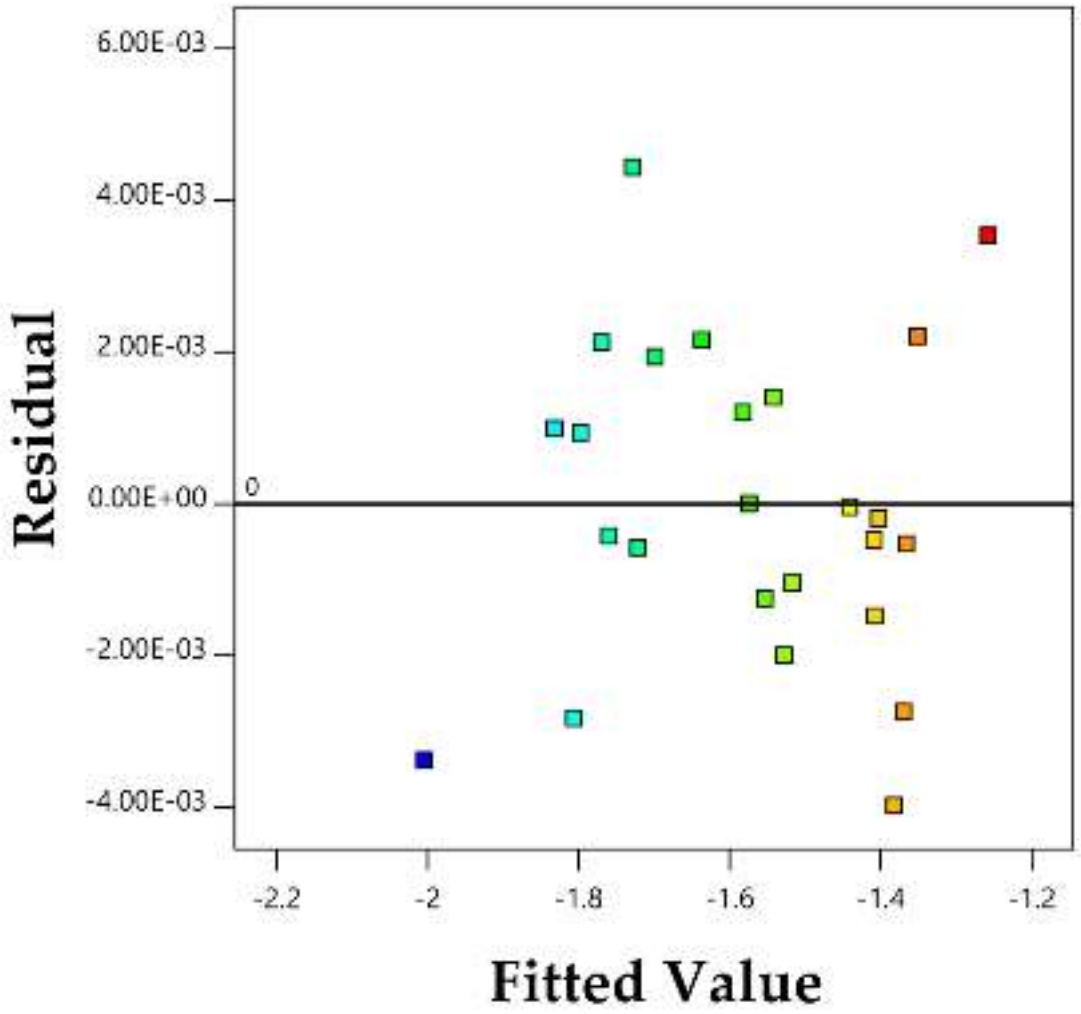

Figure 4.16: *Residual versus fitted value of* Cf_{SWCNT}

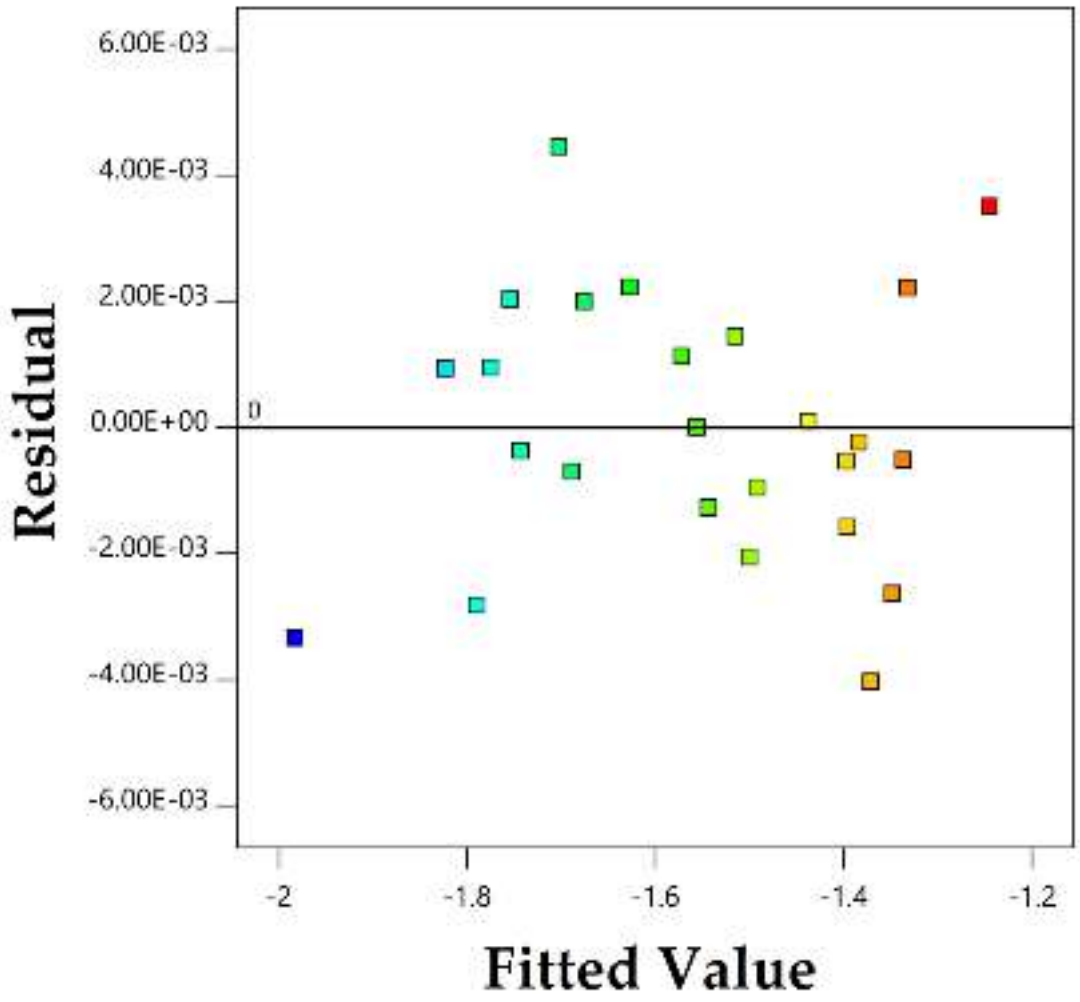

Figure 4.17: *Residual versus fitted value of* Cf_{MWCNT}

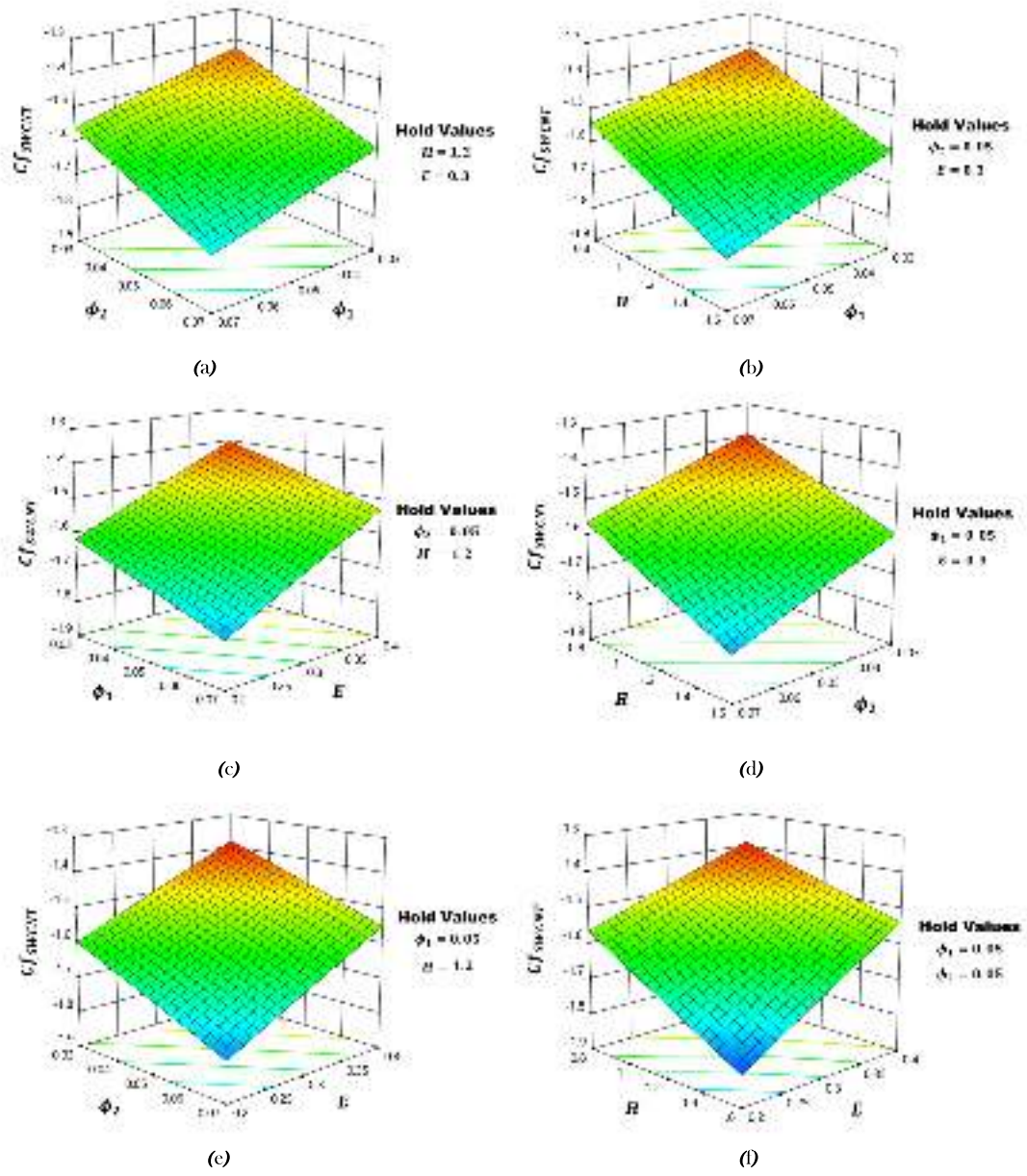

Figure 4.18: *Surface plots* Cf_{SWCNT}

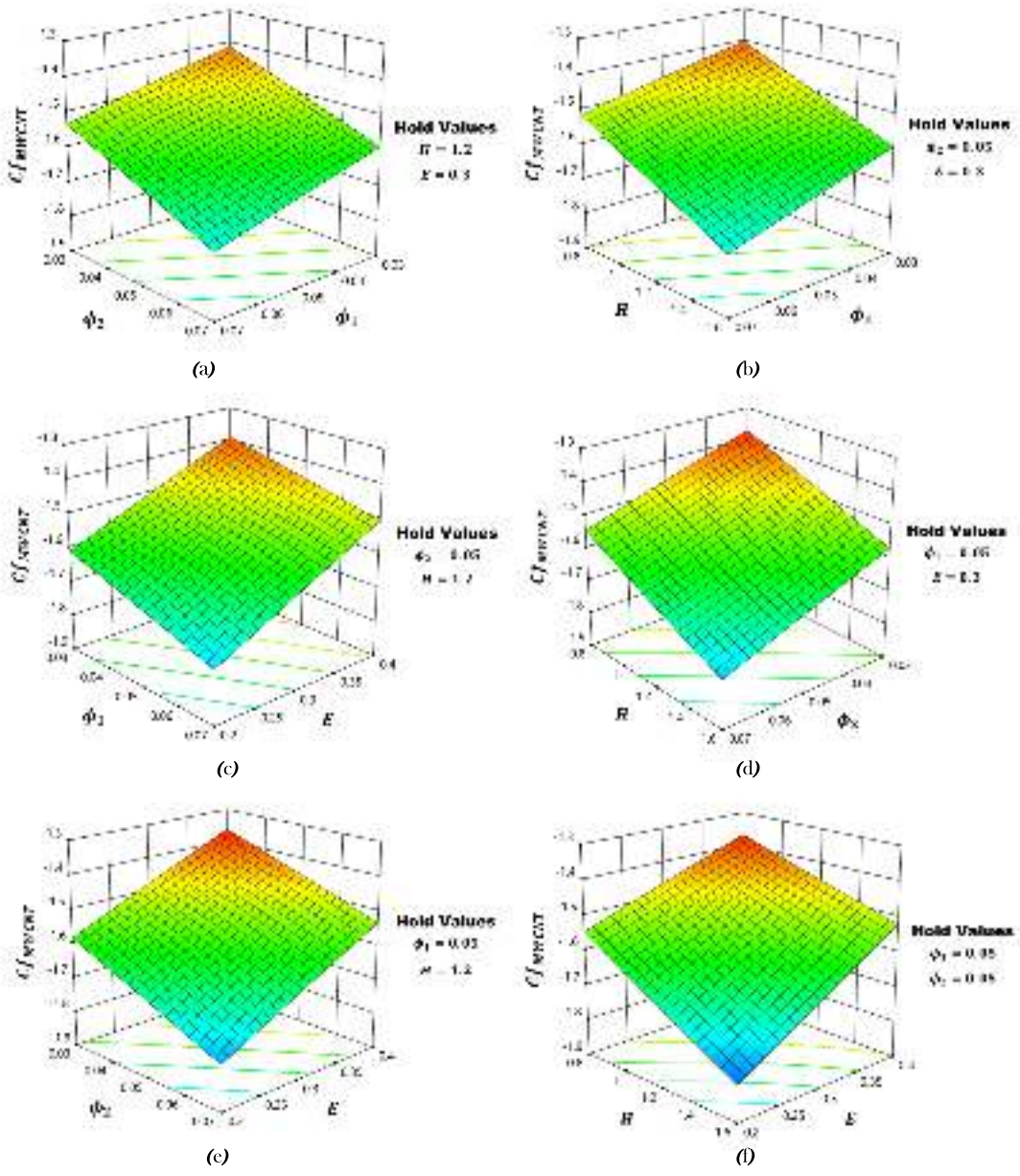

Figure 4.19: *Surface plots* Cf_{MWCNT}

APPENDIX I: Non-Dimensional Quantities

$H = (\sigma_f B_0^2)/(C_p)_f$	Hartmann Number
$E = \frac{E_0}{B_0 u_w}$	Electric Field Parameter
$Pr = \frac{\vartheta_f}{\alpha_f}$	Prandtl Number
$K_c = \frac{K_0}{c}$	Chemical Reaction Parameter
$Le = \frac{\vartheta_f}{D_B}$	Lewis Number
$Ec = \frac{(cx)^2}{((C_p)_f(T_w - T_0))}$	Eckert Number
$Lb = \frac{\vartheta_f}{D_m}$	Bioconvection Lewis Number
$Pe = \frac{bW_c}{D_m}$	Bioconvection Peclet Number
$\Omega = \frac{N_\infty}{(N_w - N_0)}$	Microorganism Concentration Difference Parameter
$S_1 = \frac{\delta_2}{\delta_1}$	Thermal Stratification Parameter
$S_2 = \frac{\varepsilon_2}{\varepsilon_1}$	Mass Stratification Parameter
$S_3 = \frac{\xi_2}{\xi_1}$	Microorganism Density Stratification Parameter

Appendix II : Nomenclature

u, v	Velocity components	T	Fluid temperature
C	Concentration of nanoparticles	μ	dynamic viscosity
T_∞	Ambient temperature	u_w	Stretching velocity
C_∞	Ambient concentration of nanoparticles	C_w	Surface concentration of nanoparticles
N_∞	Ambient concentration of Microorganism	N_w	Surface concentration of Microorganism
C_0	Reference concentration of nanoparticles	N_0	Reference concentration of Microorganism
S_3	Microorganism density stratification parameter	D_B	Brownian diffusion coefficient
ψ	Dimensionless concentration of nanoparticles	χ	Dimensionless concentration of Microorganism
θ	Dimensionless temperature	ρ	density
T_0	Reference temperature	B_0	Magnetic field strength
W_c	Maximum cell swimming speed	T_w	Surface temperature
c	Stretching rate	α	Thermal diffusivity
C_p	Specific heat	hnf	Hybrid nanofluid
D_m	Microorganisms diffusion coefficient	σ	electrical conductivity
E_0	Applied electric field	η	Dimensionless variable
N	Concentration of Microorganism	ν	kinematic viscosity
S_1	Thermal stratification parameter	s_1	CNT nanoparticle
S_2	Mass stratification parameter	s_2	Fe_3O_4 nanoparticle
ϕ_2	Volume fraction of Fe_3O_4	f	Base fluid
ϕ_1	Volume fraction of CNT	nf	Nanofluid
K_0	Chemical reaction coefficient	$\delta_1, \delta_2, \varepsilon_1, \varepsilon_2, \xi_1, \xi_2$	constants